# The X-linked intellectual disability gene product and E3 ubiquitin ligase KLHL15 degrades doublecortin proteins to constrain neuronal dendritogenesis

Received for publication, October 2, 2020, and in revised form, October 27, 2020 Published, Papers in Press, November 16, 2020,
https://doi.org/10.1074/jbc.RA120.016210

**Jianing Song**[‡], **Ronald A. Merrill**[‡], **Andrew Y. Usachev**, **and Stefan Strack**[*]

*From the Department of Neuroscience and Pharmacology and the Iowa Neuroscience Institute, University of Iowa, Iowa City, Iowa, USA*

Edited by George DeMartino

**Proper brain development and function requires finely controlled mechanisms for protein turnover, and disruption of genes involved in proteostasis is a common cause of neurodevelopmental disorders. Kelch-like 15 (KLHL15) is a substrate adaptor for cullin3-containing E3 ubiquitin ligases, and *KLHL15* gene mutations were recently described as a cause of severe X-linked intellectual disability. Here, we used a bioinformatics approach to identify a family of neuronal microtubule-associated proteins as KLHL15 substrates, which are themselves critical for early brain development. We biochemically validated doublecortin (DCX), also an X-linked disease protein, and doublecortin-like kinase 1 and 2 as *bona fide* KLHL15 interactors and mapped KLHL15 interaction regions to their tandem DCX domains. Shared with two previously identified KLHL15 substrates, a FRY tripeptide at the C-terminal edge of the second DCX domain is necessary for KLHL15-mediated ubiquitination of DCX and doublecortin-like kinase 1 and 2 and subsequent proteasomal degradation. Conversely, silencing endogenous KLHL15 markedly stabilizes these DCX domain-containing proteins and prolongs their half-life. Functionally, overexpression of KLHL15 in the presence of WT DCX reduces dendritic complexity of cultured hippocampal neurons, whereas neurons expressing FRY-mutant DCX are resistant to KLHL15. Collectively, our findings highlight the critical importance of the E3 ubiquitin ligase adaptor KLHL15 in proteostasis of neuronal microtubule-associated proteins and identify a regulatory network important for development of the mammalian nervous system.**

Ubiquitination is a highly coordinated multistep enzymatic cascade that requires the concerted action of three key factors: E1 ubiquitin-activating enzymes, E2 ubiquitin-conjugating enzymes, and E3 ubiquitin ligases (1), many of which are strongly implicated in the pathogenesis of neurodevelopmental disorders (2–4). E3 ubiquitin ligases have received particular attention, as they confer substrate specificity of the ubiquitination reaction by catalyzing the transfer of ubiquitin to proteins destined for degradation or other ubiquitin-dependent fates (5–7).

Recent studies have identified *KLHL15* as an X-linked intellectual disability (XLID) gene. Inactivating *KLHL15* mutations are associated with various brain abnormalities as well as developmental and behavioral disorders in male patients (8–11). Localized on chromosome Xp22.11, *KLHL15* encodes a member of the Kelch-like (KLHL) family of proteins that function as adaptors for cullin3 (Cul3)-based E3 ubiquitin ligases to target specific substrates to the ubiquitin-proteasome system (12). Numbering more than 40 in humans, KLHL proteins exert a wide range of biological functions, whereas genetic mutations and abnormal expression of *KLHL* genes have been linked to diverse diseases, ranging from cardiovascular disorders to cancer (12–14).

We have previously demonstrated that KLHL15 mediates the ubiquitination and subsequent proteasomal degradation of the B′$\beta$ (B56$\beta$, PR61$\beta$, PPP2R5B) regulatory subunit of the protein Ser/Thr phosphatase 2A (PP2A). KLHL15-mediated B′$\beta$ degradation facilitates the formation of alternative PP2A holoenzymes by promoting the exchange with more than a dozen other regulatory subunits (15). PP2A/B′$\beta$ is highly enriched in the mammalian nervous system (16–18) and plays key roles in striatal dopamine biosynthesis (16), hippocampal long-term potentiation (19), and multiple intracellular signaling pathways in response to growth factor stimulation (20–22). We also identified a tyrosine residue (Y52) within a phylogenetically well-conserved tripeptide motif (FRY) in vertebrate B′$\beta$ as being necessary for KLHL15 binding and KLHL15-mediated B′$\beta$ downregulation (15). Since then, work by others identified a critical FRY tripeptide in the degron of a second KLHL15 substrate, the DNA repair protein CtIP/RBBP8 (23).

Because of *KLHL15*'s link to severe intellectual disability and its ranking as one of the most clinically significant X-linked disease genes (8, 24), we set out to uncover novel neuronal substrates of the E3 ubiquitin ligase by primary and secondary structure searches. This screen and subsequent biochemical validation identified doublecortin (DCX) and two doublecortin-like kinases (DCLK1, DCLK2), members of a family of neuronal microtubule-associated proteins (MAPs) that share a characteristic domain structure of N-terminal

[‡] These authors contributed equally to this work.
[*] For correspondence: Stefan Strack, stefan-strack@uiowa.edu.

tandem DCX domains. These tandem DCX domains stabilize microtubule by enhancing tubulin polymerization, inhibiting tubulin catastrophe, and promoting microtubule bundling (25–28). DCX plays essential roles in neurogenesis, neuronal migration, axonal/dendritic wiring, and cargo transport therefore ensuring normal brain development (28, 29). The *DCX* gene is located on the X chromosome, and *DCX* mutations cause classic lissencephaly (agyria) in males and subcortical band heterotopia (also called double cortex syndrome) primarily in females as a result of neuronal migration defects (30). Both disorders typically manifest with intellectual disability, epilepsy, language impairment, and global developmental delay (30). DCLK1 and DCLK2 feature a C-terminal Ser/Thr kinase domain and play both common and distinct roles in neurodevelopment. Both kinases associate with microtubules and stimulate microtubule polymerization and dendritic development independently of their kinase activity (31–33). DCLK1 and DCX synergistically regulate neuronal migration, axonal outgrowth, and hippocampal development (34–36), whereas DCLK2 works in concert with DCX to organize hippocampal lamination and prevent spontaneous seizures (37).

This report documents that three members of the DCX family of neuronal MAPs are subject to KLHL15-mediated downregulation. KLHL15-dependent polyubiquitination and proteasomal degradation requires a degron containing both N-terminal DCX domains and a conserved FRY tripeptide. Functionally, we show that KLHL15 expression reduces dendritic arborization in primary hippocampal cultures unless neurons also express DCX with a stabilizing FRY mutation. Our study uncovers a novel role of the E3 ubiquitin ligase adaptor KLHL15 as a negative regulator of DCX protein abundance and dendritogenesis and suggests possible mechanistic connections in X-linked neurodevelopmental disorders.

## Results

### *KLHL15 regulates signal transduction in hippocampal neurons by PP2A-dependent and independent mechanisms*

Two KLHL15 substrates have been identified to date, the neuron-enriched PP2A regulatory subunit B′$\beta$ (15) and CtIP/RBBP8, a widely expressed endonuclease involved in DNA repair by homologous recombination (23). According to gene expression databases (e.g., https://www.ebi.ac.uk/gxa), B′$\beta$ is more highly expressed in the adult than in the embryonic human brain. This raises the question whether this PP2A subunit is relevant for the neurodevelopmental consequences of *KLHL15* mutations.

To determine whether KLHL15 possesses functions in neurons independent of PP2A/B′$\beta$, we investigated the effect of KLHL15 on activation of extracellular signal-regulated kinases (ERKs, Fig. 1*A*). We previously reported that the B′$\beta$-containing PP2A holoenzyme potentiates nerve growth factor signaling at the tropomyosin-related kinase A (TrkA) receptor level to sustain ERK signaling and neuronal differentiation of neuroendocrine PC12 cells (22). To address the hypothesis that PP2A/B′$\beta$ may similarly potentiate TrkB receptor activity in central neurons, we measured ERK activity in transiently transfected primary hippocampal neurons from E18 rat embryos using a dual luciferase reporter assay (PathDetect Elk1 reporter, Fig. 1*A*) (22). In GFP control-transfected neurons, a 3-h incubation with a subsaturating concentration of brain-derived neurotrophic factor (BDNF) resulted in a several-fold increase in Elk1 transcriptional activity (Fig. 1*B*). Compared with control, overexpression of GFP-KLHL15 attenuated ERK activation by 2.5-fold, whereas B′$\beta$ overexpression amplified the BDNF response by 3-fold (Fig. 1*B*). Conversely, silencing of endogenous KLHL15 amplified BDNF signaling to ERK by 1.5-fold over control shRNA-transfected cells, whereas shRNA targeting endogenous B′$\beta$ nearly eliminated the BDNF response (Fig. 1*C*). These results suggest that KLHL15 inhibits neurotrophin signaling in hippocampal neurons primarily by targeting PP2A/B′$\beta$ for proteasomal degradation. The neuromodulator pituitary adenylate cyclase-activating polypeptide (PACAP) signals through the type 1 G protein–coupled receptor PAC1 to ERK via cAMP-dependent activation of Rap1 (38) (Fig. 1*A*). In control-transfected neurons, PACAP at subsaturating concentration induced Elk1 transcriptional activity by ∼5-fold (Fig. 1*D*). Overexpression of GFP-KLHL15 dampened this response by ∼2-fold, whereas KLHL15 silencing amplified PACAP signaling to ERK by ∼3-fold (Fig. 1, *D*–*E*). In contrast to BDNF stimulation, neither overexpression nor knockdown of PP2A/B′$\beta$ significantly affected the reporter response to PACAP (Fig. 1, *D*–*E*), suggesting the involvement of a distinct KLHL15 substrate.

### *A sequence and structure search identifies DCX and DCLK1/2 as potential KLHL15 substrates*

To uncover additional neuronal KLHL15 substrates, we searched the human UniProt database for proteins that contain the FRY sequence, which is necessary for the interaction of KLHL15 with its two previously identified targets, PP2A/B′$\beta$ (15) and the DNA endonuclease CtIP/RBBP8 (23). This search identified a list of 616 proteins, which was further narrowed down according to secondary structure prediction (Fig. 2*A*). The FRY sequence in B′$\beta$ and CtIP/RBBP8 is predicted to adopt a β-strand flanked by extended unstructured regions, which we reasoned provides flexibility for protein–protein interactions. Constraining the list of FRY-containing proteins to those in which the tripeptide is within a 2- to 4-residue-long β-strand surrounded by at least five unstructured residues on both sides yielded a list of 24 proteins (Fig. 2*A*), which includes signaling proteins, transcription factors, and proteins involved in proteostasis (Table 1). We focused on three proteins: DCX and two doublecortin-like kinases DCLK1 and DCLK2, which belong to a group of 11 neuronal MAPs characterized by microtubule binding, tandem DCX domains that function during brain development (25, 33–37, 39). The FRY tripeptide is situated at the extreme C-terminal border of the second DCX domain (Fig. 2*B*). This region is highly conserved with the FRY sequence present in all vertebrate orthologs of DCX, DCLK1, and DCLK2. The region is not conserved in DCLK3, an atypical and largely

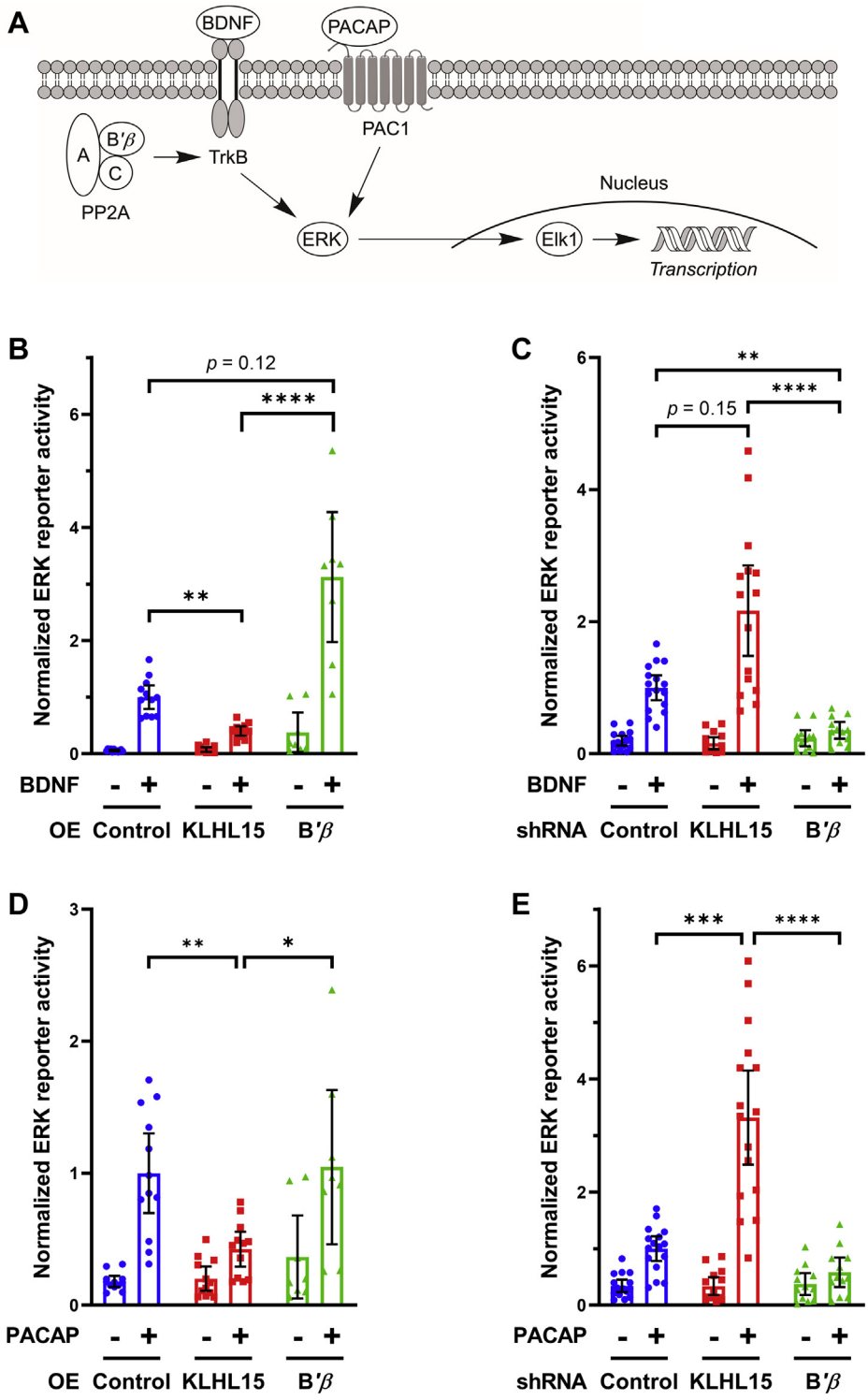


**Figure 1. KLHL15 modulates BDNF- and PACAP-mediated ERK activation in hippocampal neurons by different mechanisms.** *A*, schematic of BDNF and PACAP signaling resulting in Elk1-mediated luciferase activity as a reporter of ERK activation. *B–D*, hippocampal cultures from E18 rat embryos transfected with the indicated cDNAs or shRNAs together with dual-luciferase reporter plasmids (PathDetect Elk1 reporter) were stimulated (+) with BDNF (25 ng/ml) or PACAP (10 nM) for 3 h prior to lysis and luminometry. Luciferase activities were normalized to the treatment response of the control. *B* and *C*, BDNF responses were enhanced by knockdown of KLHL15 and overexpression (OE) of B′*β* but diminished by KLHL15 overexpression or B′*β* knockdown. *D* and *E*, PACAP-stimulated ERK activities were modulated by KLHL15 but insensitive to B′*β* manipulation. Data points are values from individual wells of two to four independent experiments; also shown are means ± 95% confidence interval (CI). Data of the stimulated (+) conditions were analyzed by Kruskal–Wallis tests with Dunn's multiple comparisons tests. *$p < 0.05$, **$p < 0.01$, ***$p < 0.001$, and ****$p < 0.0001$.

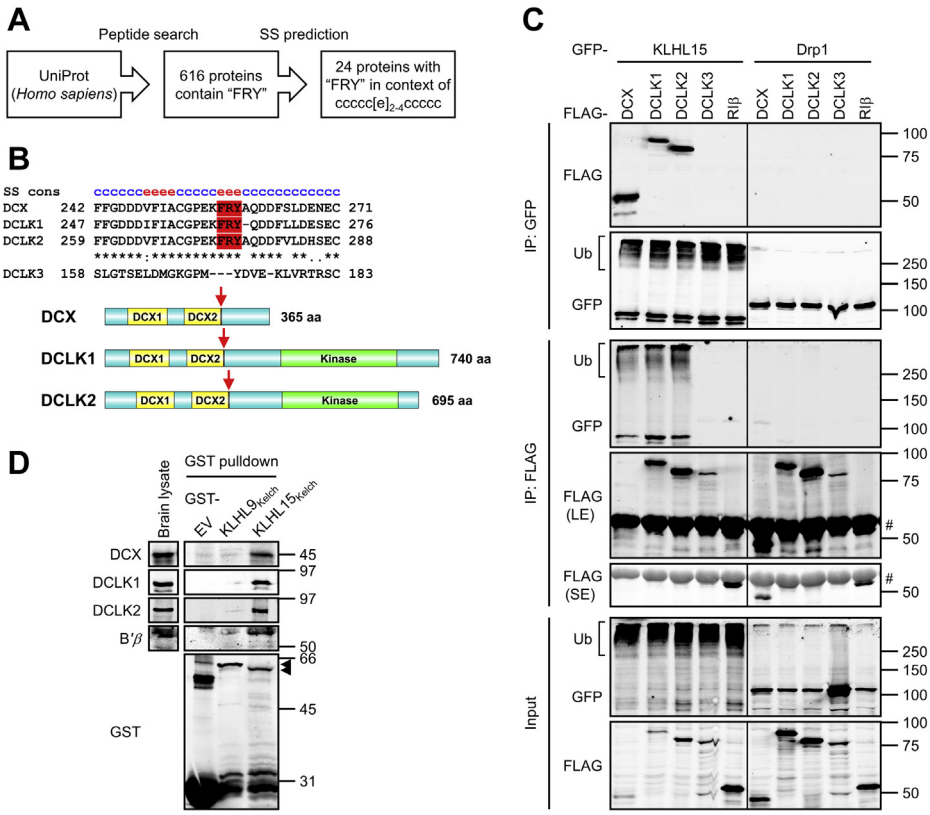


**Figure 2. KLHL15 interacts with DCX, DCLK1, and DCLK2.** *A*, search strategy for putative KLHL15 substrates. The human UniProt database was first screened for proteins containing the FRY sequence. The resulting 616 proteins were analyzed by consensus secondary structure (SS) prediction (https://npsa-prabi.ibcp.fr/) and filtered for proteins in which the FRY sequence is centered in the listed secondary structure (c, random coil; e, β-strand), yielding the 24 proteins listed in Table 1. *B*, on top is a multiple sequence alignment of human DCX (UniProt ID: O43602-1), DCLK1 (UniProt ID: O15075-1), DCLK2 (UniProt ID: G5E9L9) with FRY sequence in *red* and consensus secondary structure (cons SS) above. Because of insufficient homology, DCLK3 (UniProt ID: Q9C098) was aligned manually. Domain diagrams with *red arrows* indicating the FRY sequence are shown at the bottom. *C*, GFP-tagged KLHL15 was coexpressed with FLAG-tagged DCX, DCLK1, DCLK2, or DCLK3 in COS-1 cells, and KLHL15–substrate interaction was assessed by reciprocal immunoprecipitation (IP) via GFP or FLAG epitope tag and immunoblotting with the indicated antibodies. GFP-Drp1 and FLAG-RIβ were included as a negative control for GFP or FLAG protein, respectively. Western blots representative of four independent experiments are shown. *D*, bacterially expressed GST, GST-KLHL9$_{Kelch}$, or GST-KLHL15$_{Kelch}$ protein was incubated with a whole brain lysate from E18 rat embryos, and association of endogenous proteins was evaluated by GST pulldown and immunoblotting with the indicated antibodies. Western blots representative of three independent experiments are shown. *Arrows* point to the full-length GST-KLHL9$_{Kelch}$ and GST-KLHL15$_{Kelch}$ proteins. Molecular mass marker positions are indicated in kilodaltons. # indicates IgG heavy chain. LE, long exposure; SE, short exposure; Ub, polyubiquitinated species.

uncharacterized member of the DCX family, whose homology to DCLK1 and DCLK2 is largely confined to the kinase domain (40).

### *KLHL15 interacts with DCX, DCLK1, and DCLK2*

To test whether DCX, DCLK1, and DCLK2 are KLHL15 interactors, we coexpressed GFP-tagged KLHL15 and FLAG-tagged DCX or DCLKs in COS-1 cells and conducted reciprocal immunoprecipitation (IP) experiments. GFP-IP of KLHL15 selectively enriched DCX, DCLK1, and DCLK2, but not DCLK3 or another negative control (FLAG-RIβ). Similarly, only FLAG-IPs of DCX and DCLK1/2 isolated GFP-KLHL15 (Fig. 2*C*). No interactions were detected with dynamin-related protein 1 (GFP-Drp1), indicating that DCX and DCLK1/2 do not interact with GFP. Notably, compared with GFP-Drp1, coexpression of GFP-KLHL15 dramatically decreased steady-state levels of the three interacting proteins (Fig. 2*C*, input).

To obtain evidence for direct interactions with endogenous proteins, we performed glutathione-*S*-transferase (GST) pulldown experiments with brain lysates from E18 rat embryos. A GST fusion of the substrate-binding Kelch domain of KLHL15 (amino acids 255–604, GST-KLHL15$_{Kelch}$ [15]) was able to capture the endogenous PP2A/B'$\beta$ regulatory subunit, as well as DCX, DCLK1, and DCLK2 (Fig. 2*D*). Indicating specificity for KLHL15, none of the proteins were pulled down with the Kelch domain of KLHL9 (GST-KLHL9$_{Kelch}$) or GST alone (EV, Fig. 2*D*).

### *The tandem DCX domains are necessary and sufficient for KLHL15 binding*

To map the KLHL15-binding domain of DCX proteins, we constructed chimeras between the interactor DCLK2 and the non-interactor DCLK3. Chimera DCLK3-2 is composed of the N terminus of DCLK3 (amino acids 1–130) and C terminus of DCLK2 (amino acids 236–695), including the FRY tripeptide and the C-terminal half of the second DCX domain (Fig. 3*A*). DCLK2-3 is a chimera between the DCLK2 N terminus (amino acids 1–281; including the DCX1 and DCX2 domain tandem) and the C-terminal Ser/Thr kinase domain of DCLK3 (amino

**Table 1**
**List of 24 putative KLHL15 substrates identified by the two-step *in silico* screen**

| Protein | Annotation |
|---|---|
| ATXN2 | RNA stability regulator Ataxin-2/SCA2 |
| AXIN1 | β-Catenin destruction complex component Axin-1 |
| CACNG8 | Voltage-dependent calcium channel γ8 subunit |
| CADH3 | Cadherin-3 |
| DCLK1 | Serine/threonine-protein kinase DCLK1 |
| DCLK2 | Serine/threonine-protein kinase DCLK2 |
| DCX | Neuronal migration protein doublecortin |
| DIXDC1 | Wnt signaling pathway effector Dixin |
| DUSP2 | Dual specificity protein phosphatase 2 |
| EPB41L2 | Erythrocyte membrane protein band 4.1 like 2 |
| HERC4 | Probable E3 ubiquitin-protein ligase HERC4 |
| PDE8 | Cyclic nucleotide phosphodiesterase 8B |
| PDZD8 | PDZ domain-containing protein 8 |
| PPP2R5B | Protein phosphatase 2A regulatory subunit B′β |
| PPIAL4C | Peptidyl-prolyl cis-trans isomerase A-like 4C |
| PSMG2 | Proteasome assembly chaperone 2 |
| PTPN4 | Tyrosine-protein phosphatase non-receptor type 4 |
| RABL6A | RAB-like GTPase RABL6A |
| RBBP8 | DNA endonuclease RBBP8/CtIP |
| TCF20 | Transcription factor 20 |
| TMEM161A | Transmembrane protein 161A |
| TRPS1 | Zinc finger transcription factor Trps1 |
| USPL1 | SUMO-specific isopeptidase USPL1 |
| ZFP37 | Zinc finger protein 37 |

acids 176–648, Fig. 3*A*). According to IP experiments with transfected COS-1 cells, GFP-KLHL15 immunoisolated comparable levels of DCLK2 and DCLK2-3 (Fig. 3*B*, labeled FL, full length). In contrast, DCLK3-2 was not detectable in the GFP-KLHL15 IP. These data indicate that $DCLK2_{1\text{-}281}$ mediates the interaction with KLHL15 and that residues 236 to 281 including the FRY sequence are not sufficient for binding.

To further narrow down the KLHL15 docking region within the DCLK2 N terminus, we generated N-terminal truncations in the context of the DCLK2-3 chimeric cDNA (Fig. 3*A*). Deleting 50 amino acids from the unstructured N terminus did not compromise the association with GFP-KLHL15 (Fig. 3*B*, compare lanes FL and ΔN50). Truncations into the first DCX domain (ΔN117) and beyond (ΔN179, ΔN209), in contrast, eliminated KLHL15 binding (Fig. 3*B*). Thus, DCLK2 residues 51 to 281 including both DCX domains are necessary and sufficient for the KLHL15 interaction. These mapping results likely also apply to DCX and DCLK1, in which this region is 80% and 82% identical, respectively.

### *Tyr within the FRY sequence of DCX proteins is critical for KLHL15-mediated polyubiquitination and degradation*

Point mutations within the FRY sequences of B′β and CtIP/RBBP8 disrupt interactions with KLHL15 (15, 23). To evaluate whether this also holds true for DCX proteins, we generated Tyr to Leu substitutions within their FRY sequences. Indeed, DCX-Y259L, DCLK1-Y265L, and DCLK2-Y276L displayed significantly decreased KLHL15 binding in IPs (∼10%–20% of their WT counterparts, Fig. 4, *A*–*B*), highlighting the critical importance of the Tyr residue in the FRY sequence. Residual KLHL15 binding of the mutant proteins is likely a consequence of their increased steady-state levels (Fig. 4*A*, input).

We next tested whether KLHL15 binding mediates polyubiquitination of the DCX proteins, first in an intact-cell context. COS-1 cells were cotransfected with HA-tagged ubiquitin, GFP-tagged KLHL15, and FLAG-tagged WT or FRY-mutant DCX and treated with proteasome inhibitor MG132 to allow accumulation of ubiquitinated proteins. Polyubiquitinated species of DCX were concentrated by FLAG-IP and probed with a DCX-specific antibody. Compared with GFP-Drp1, overexpression of KLHL15 promoted robust DCX ubiquitination (Fig. 4*C*). Polyubiquitination was substantially reduced by the Y259L mutation, despite higher levels of the unmodified, mutant protein in the IP (Fig. 4*C*), again underscoring the importance of the FRY sequence for substrate recognition and ubiquitin transfer by KLHL15.

Next, we inquired whether the Cul3–KLHL15 E3 ubiquitin ligase can catalyze DCX ubiquitination *in vitro*. To this end, the ubiquitination reaction was reconstituted by combining Myc-tagged ubiquitin, E1 ubiquitin-activating enzyme, E2 ubiquitin-conjugating enzyme, and immunopurified Cul3–KLHL15 E3 ubiquitin ligase with bacterially expressed DCX-HaloTag fusion protein (WT or Y259L mutant) and initiated by the addition of ATP. Incubation of Cul3–KLHL15 E3 ligase with the WT DCX protein induced robust and time-dependent DCX polyubiquitination. In contrast, ubiquitination of DCX-Y259L was strongly impaired under these conditions (Fig. 4, *D*–*E*), demonstrating that the Cul3–KLHL15 E3 ubiquitin ligase catalyzes DCX ubiquitination in a Y259-dependent manner.

To investigate DCX protein turnover and its dependence on KLHL15 and the FRY sequence, we analyzed substrate protein degradation using a HaloTag-based pulse-chase protocol, which we recently developed for long-lived proteins (41). HEK293T cells expressing endogenous KLHL15 (15) were cotransfected with DCX-HaloTag fusion cDNAs (WT or Y259L) and either GFP-KLHL15 or KLHL15-directed shRNAs (15), followed by pulse-labeling with a cell-permeant and covalent HaloTag ligand coupled to the fluorophore tetramethyl rhodamine (TMR). Labeled DCX-HaloTag was chased by incubating cells with the non-fluorescent competitive ligand 7-bromoheptanol for up to 24 h (41). DCX turnover was quantified by dividing TMR fluorescence by DCX immunoblot signals in the same lane and normalizing to the zero time point. Silencing endogenous KLHL15 with two different shRNAs increased steady-state levels of WT DCX-HaloTag (TMR labeling without chase) and markedly slowed its turnover ($t_{1/2}$ > 24 h versus $t_{1/2}$ = 16 h, from monoexponential decay curve fits). In contrast, KLHL15 silencing did not further stabilize the already long-lived Y259L-mutant DCX (all $t_{1/2}$ > 24 h; Fig. 5, *A*–*B*). Conversely, overexpression of GFP-KLHL15 lowered WT DCX steady-state levels and accelerated DCX turnover ($t_{1/2}$ = 5 h; Fig. 5, *A*–*B*), while having minimal effects on turnover of the FRY-mutant protein ($t_{1/2}$ = 20 h; Fig. 5, *A*–*B*). Statistical analyses of areas under the degradation curves (area under the curve [AUC]s, Fig. 5*C*) confirmed our identification of KLHL15 as a critical determinant of DCX stability and the importance of the FRY tripeptide.

We similarly examined the turnover of the two DCX domain-containing protein kinases using HaloTag pulse-chase labeling in HEK293T cells. With half-lives of greater than 24 h, both DCLK1 (Fig. 6) and DCLK2 (Fig. 7) were significantly

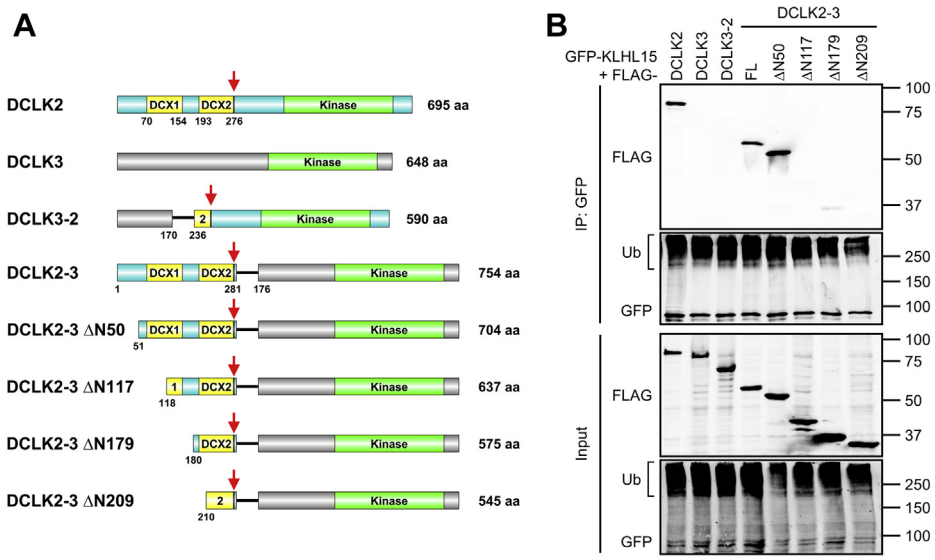


**Figure 3. The minimal KLHL15 docking region of DCLK2 includes both DCX domains.** *A*, domain diagrams of DCLK2, DCLK3, and full-length or truncated DCLK chimeras. *Red arrows* mark the locations of the FRY sequence. *B*, GFP-tagged KLHL15 was coexpressed with the indicated FLAG-tagged DCLK constructs in COS-1 cells, and interactions were analyzed by GFP-IP and probing for FLAG. Shown are Western blots representative of four independent experiments. Molecular mass marker positions are shown in kilodaltons. FL, full length; Ub, polyubiquitinated species.

more stable than DCX (greater AUCs, $p < 0.0001$). Nonetheless, forced expression of GFP-KLHL15 promoted degradation of both DCLK1 ($t_{1/2}$ = 10 h) and DCLK2 ($t_{1/2}$ = 18 h), whereas endogenous KLHL15 silencing further stabilized the DCX-domain kinases as evidenced by AUC analyses (Figs. 6*C* and 7*C*). Just like DCX-Y259L, the KLHL15-binding-impaired DCLK1-Y265L and DCLK2-Y276L mutants were not further stabilized by KLHL15 silencing. As well, turnover of mutant DCLK1/2 was less sensitive to KLHL15 overexpression than turnover of their WT counterparts (AUCs, $p < 0.01$). In aggregate, these data indicate that protein stability of DCX, DCLK1, and DCLK2 is controlled by KLHL15 in a FRY-dependent manner.

### *KLHL15 negatively regulates dendritic complexity of hippocampal neurons*

DCX is an abundant microtubule-binding protein in the developing brain, whose loss of function leads to severe neurological deficits in humans (28, 42). To examine the interplay between the two XLID genes *DCX* and *KLHL15* in a model of neuronal development, we quantified dendritic complexity of primary hippocampal neurons cultured from E18 rat embryos. Two days after plating, cultures were transfected with membrane-targeted mCherry (Lck-mCherry) to visualize neurites, together with GFP-KLHL15 and either WT or FRY-mutant DCX, or empty vector (GFP, EV) controls. Three days later, neurons were fixed, imaged, and dendritic trees were traced semiautomatically for total length and Sholl analysis (representative images in Fig. 8*A*). The expression of either WT or mutant DCX alone resulted in a slight, but non-significant increase in total dendritic intersections and total dendrite length compared with the control (Fig. 8, *B–E*), likely due to a ceiling effect of high endogenous DCX levels in these embryonic cultures. However, coexpression of GFP-KLHL15 with WT DCX dramatically reduced dendritic complexity and length (Fig. 8, *B*, *D*, and E). Dendritic growth stunted by KLHL15 could be completely reversed by coexpressing the KLHL15-resistant DCX-Y259L mutant protein (Fig. 8, *C–E*). These results suggest that KLHL15 restricts process formation in embryonic neurons by targeting DCX for proteasomal degradation.

## Discussion

Ubiquitin-processing enzymes are fundamental for neuronal development and function (43, 44) and dysregulation of these enzymes can cause neurodevelopmental (2, 3, 45) and neurodegenerative diseases (4, 46). E3 ligases determine the substrate specificity of the ubiquitination reaction, as they directly interact with proteins targeted for ubiquitination (47). Among >600 predicted human E3 ligases, cullin-RING ligase (CRLs) constitute the largest family, regulating a plethora of biological pathways (48, 49). In fact, mutations in many CRL genes are strongly associated with neurodevelopmental disorders (5–7, 50).

Among the cullin3-based CRLs, E3 ubiquitin ligases of the KLHL (BTB-Kelch) family catalyze the formation of predominantly lysine 48-linked ubiquitin chains that trigger proteasomal degradation (12–14). Many *KLHL* genes have been implicated in carcinogenesis and hereditary disorders (12), and loss of function of *KLHL15*, the subject of the present study, is associated with severe XLID (8).

Here, we used an *in silico* approach to identify novel substrates of KLHL15 important for early brain development. Our results show that KLHL15 interacts with and targets 3 of the 11 members of the doublecortin family of neuronal MAPs (DCX, DCLK1, and DCLK2) for ubiquitination and subsequent proteasomal degradation. Identified now in a total of five KLHL15 targets, including the PP2A regulatory subunit B'$\beta$

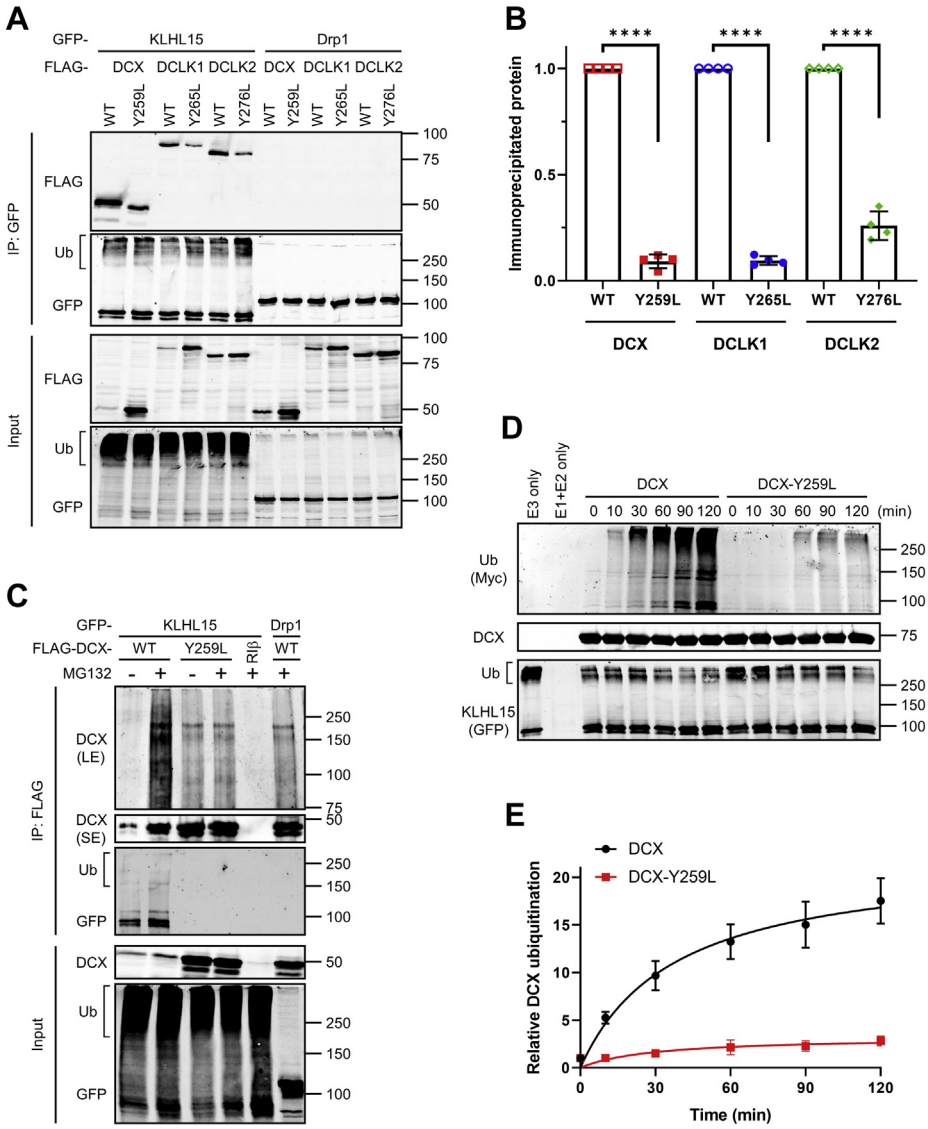


**Figure 4. The FRY sequence of DCX is critical for KLHL15 binding and KLHL15-mediated polyubiquitination in cells and *in vitro*.** *A*, GFP-tagged KLHL15 or Drp1 was coexpressed with FLAG-tagged DCX, DCLK1, or DCLK2, either WT or FRY-mutant in COS-1 cells, and interaction was assessed by GFP-IP and immunoblotting with the indicated antibodies. *B*, relative DCX (or DCLK) level after IP was quantified by dividing IP'd FLAG signals to IP'd GFP signals and then to FLAG signals in the corresponding input lane ($FLAG^{IP}/GFP^{IP}/FLAG^{Input}$) and normalizing to the WT group. Shown are means ± SD as well as individual data points from four independent experiments. $^{****}p < 0.0001$ by Student *t* test. *C*, COS-1 cells coexpressing GFP-tagged KLHL15 and FLAG-tagged DCX-WT or Y259L were treated with and without the proteasome inhibitor MG132, and lysates were subjected to FLAG-IP followed by immunoblotting with the indicated antibodies. GFP-Drp1 and FLAG-RIβ were included as a negative control for GFP or FLAG protein, respectively. The unmodified DCX was detected by a short exposure (SE), whereas polyubiquitinated DCX was visualized by long exposure (LE). Shown are Western blots representative of four independent experiments. *D*, Myc-tagged ubiquitin and purified E1/E2 enzymes were mixed with immunoisolated Cul3–KLHL15 E3 ubiquitin ligase and bacterially expressed DCX-HaloTag-$His_6$ protein (WT or Y259L), and *in vitro* ubiquitination reactions (37 °C for the indicated times) were initiated by addition of ATP. Molecular mass marker positions are shown in kilodaltons. *E*, the time course of *in vitro* DCX ubiquitination was quantified by dividing Myc signals to DCX signals and GFP signals in the same lane (Myc/DCX/GFP) and normalizing to the zero time point (set as 1). Data are shown as means ± SD from four independent experiments and were fitted to the Michaelis–Menten curve using GraphPad Prism.

and the DNA repair protein CtIP/RBBP8 (15, 23), a FRY tripeptide embedded within a predicted unstructured region is required for recognition of the three DCX domain-containing proteins by the E3 ligase.

The KLHL15 binding domain, or degron, we identified in DCX (residues 51 to 281) encompasses the FRY sequence at its C-terminal end, and also the protein-family defining, tandem DCX domains, which have been shown to stabilize the microtubule cytoskeleton by binding selectively to 13 protofilament-containing microtubules (51–53). The overlap between microtubule- and KLHL15-binding domains of DCX suggests the possibility of competitive interactions; for instance, KLHL15 may only ubiquitinate DCX proteins that are not bound to microtubules.

DCX is developmentally regulated in the mammalian brain with high expression in embryonic stages followed by a sharp decline in adulthood (54–59). DCX is also known to have heterogenous subcellular distributions in various neuronal cell types. DCX is particularly enriched at the ends of neuronal

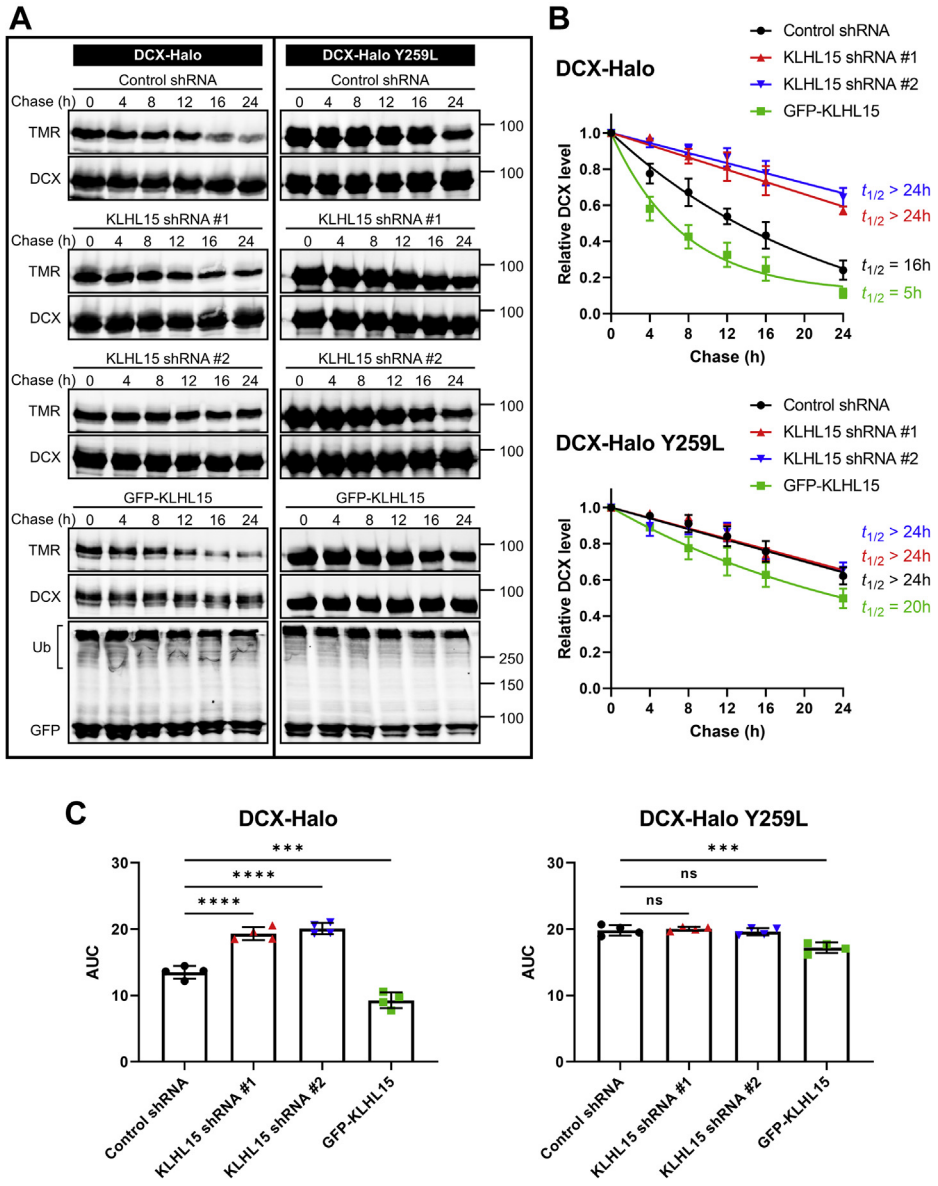


**Figure 5. KLHL15 promotes DCX protein turnover in a FRY-dependent manner.** HEK293T cells were cotransfected with DCX-HaloTag (WT or Y259L) and either the indicated shRNA plasmids or GFP-KLHL15. DCX-HaloTag was pulse-labeled (30 min, 50 nM) with tetramethyl rhodamine (TMR) fluorescent ligand and then chased with the non-fluorescent ligand 7-bromoheptanol for the indicated times before cells were lysed in SDS. *A*, total lysate blots of cells expressing WT (*left*) or mutant (*right*) DCX-HaloTag were first imaged for TMR fluorescence and then immunoblotted for DCX and GFP. Molecular mass marker positions are shown in kilodaltons. *B*, DCX degradation was quantified by dividing TMR fluorescence by DCX immunoblotting signals in the same lane (TMR/DCX) and normalizing to the zero time point. Data points are means ± SD from four independent transfections; half-lives ($t_{1/2}$) were determined from the shown one-phase decay curve fits. *C*, AUC was quantified from the decay curves in *B* and is plotted as individual data points and means ± SD from four independent experiments. *p* Values were obtained by one-way ANOVA followed by Dunnett's post hoc tests for multiple comparisons to the control shRNA group. ***$p < 0.001$, ****$p < 0.0001$. AUC, area under the curve.

processes where microtubules enter the growth cone (60) and axonal segments that can generate collaterals (61). Moreover, DCX is further involved in nuclear translocation during neuroblast migration and may influence neuroblast differentiation (62). Distinct patterns of expression and localization strongly implicate the spatiotemporal regulation of DCX via the ubiquitin-proteasome pathway. DCX's two paralogs, DCLK1 and DCLK2, also display developmental stage-specific expression and preferentially localize to distal dendrites to promote their growth by enhancing microtubule bundling (33), implying similar proteolytic regulation of the DCX domain-containing kinases.

DCX-domain proteins are likely targeted by multiple E3 ligases that are themselves differentially expressed and localized. Indeed, the nuclear E3 ubiquitin ligase Mdm2 has been reported to ubiquitinate and degrade DCX in newborn olfactory bulb interneurons (63). Mechanisms for DCX stabilization have also been documented. For instance, the 14-3-3ε protein binds and protects DCX from ubiquitination and subsequent degradation (64), whereas the deubiquitinating enzyme USP9X binds DCX in a ubiquitination-independent manner (57).

Reporter assays in hippocampal neurons point to KLHL15 as a potent negative regulator of BDNF/TrkB and PACAP/

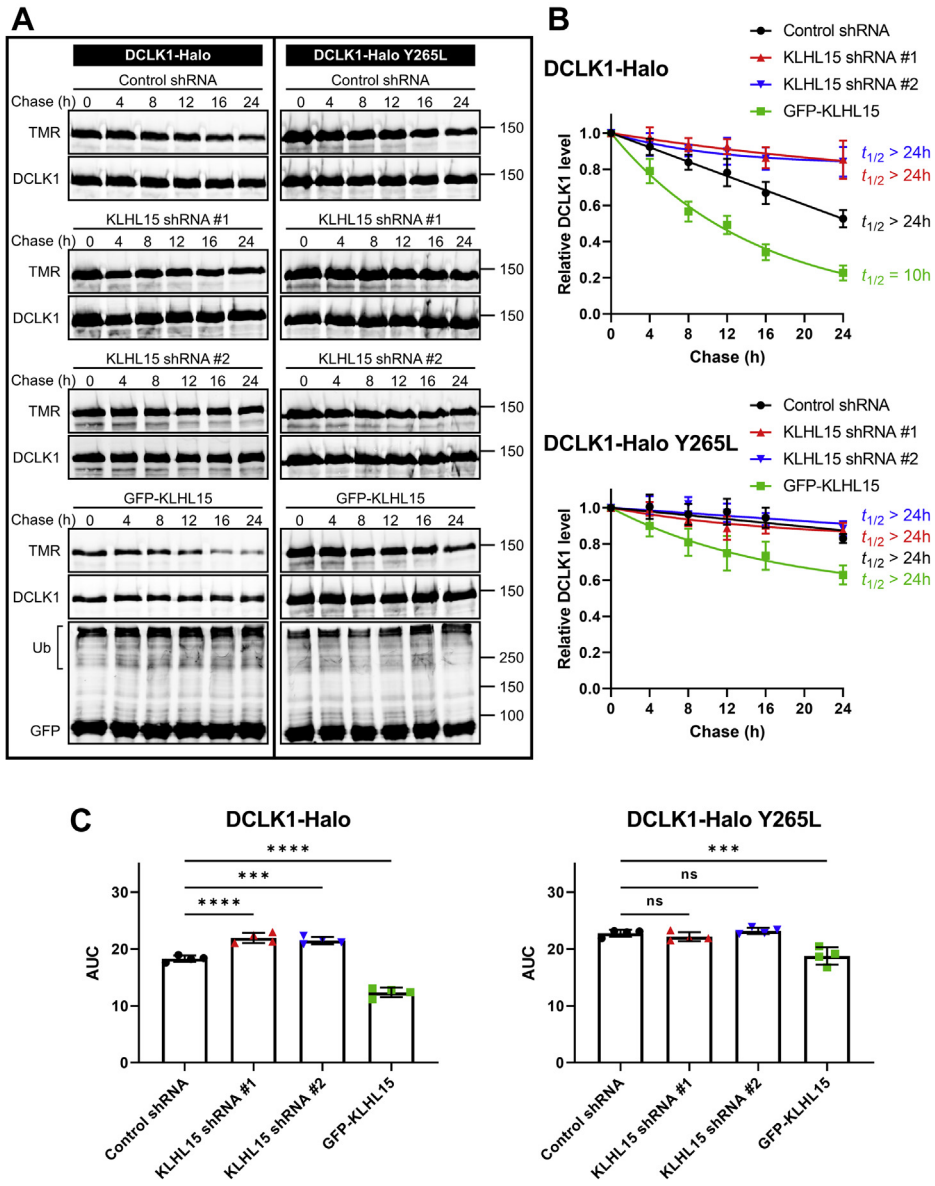


**Figure 6. KLHL15 accelerates DCLK1 degradation in a Y265-dependent manner.** HEK293T cells were cotransfected with DCLK1-HaloTag (WT or Y265L) and either GFP-KLHL15 or the indicated shRNA plasmids. DCLK1-HaloTag was pulse labeled (30 min, 50 nM) with TMR fluorescent ligand and then chased with the non-fluorescent ligand 7-bromoheptanol for the indicated times before cell lysis. *A*, total lysate blots of cells expressing WT (*left*) or mutant (*right*) DCLK1-HaloTag were first imaged for TMR fluorescence and then immunoblotted for DCLK1 and GFP. Molecular mass marker positions are shown in kilodaltons. *B*, DCLK1 degradation was quantified by dividing TMR fluorescence by DCLK1 immunoblotting signals in the same lane (TMR/DCLK1) and normalizing to the zero time point. Data points are means ± SD from four independent transfections; half-lives ($t_{1/2}$) were determined from the shown one-phase decay curve fits. *C*, AUC was quantified from the decay curves in *B* and is plotted as individual data points and means ± SD from four independent experiments. Data were analyzed by one-way ANOVA followed by Dunnett's post hoc tests for multiple comparisons to the control shRNA group. ***$p < 0.001$, ****$p < 0.0001$. AUC, area under the curve.

PAC1 signaling to ERK (Fig. 1). Knockdown and overexpression of the KLHL15 target B'$\beta$ suggests that KLHL15-mediated inhibition of TrkB signaling likely occurs via degradation of PP2A/B'$\beta$, a neuronal protein phosphatase that we previously reported amplifies nerve growth factor/TrkA signaling in PC12 cells (22). On the other hand, PACAP-mediated ERK stimulation is inhibited by KLHL15 independently of this PP2A regulatory subunit. Although DCX-domain kinases have previously been reported to modulate transcriptional response (40), it is unclear whether DCX proteins or other, as yet to be identified substrates of the E3 ligase mediate KLHL15's effects on PACAP signaling.

DCX plays pivotal roles in neurogenesis, neuronal migration, and process outgrowth to establish cortical and hippocampal lamination during early brain development (28, 29). In particular, DCX knockout or RNAi-mediated silencing impairs neurite outgrowth in developing cortical and hippocampal neurons (42, 65). Consistent with DCX stabilizing dendritic microtubules and KLHL15 targeting DCX for proteasomal degradation, we found that overexpression of KLHL15 reduces dendritic complexity in hippocampal neurons expressing WT but not FRY-mutant DCX (Fig. 8).

*DCX*-inactivating mutations cause severe structural brain abnormalities (30), whereas the case for *DCLK1* and *DCLK2* as

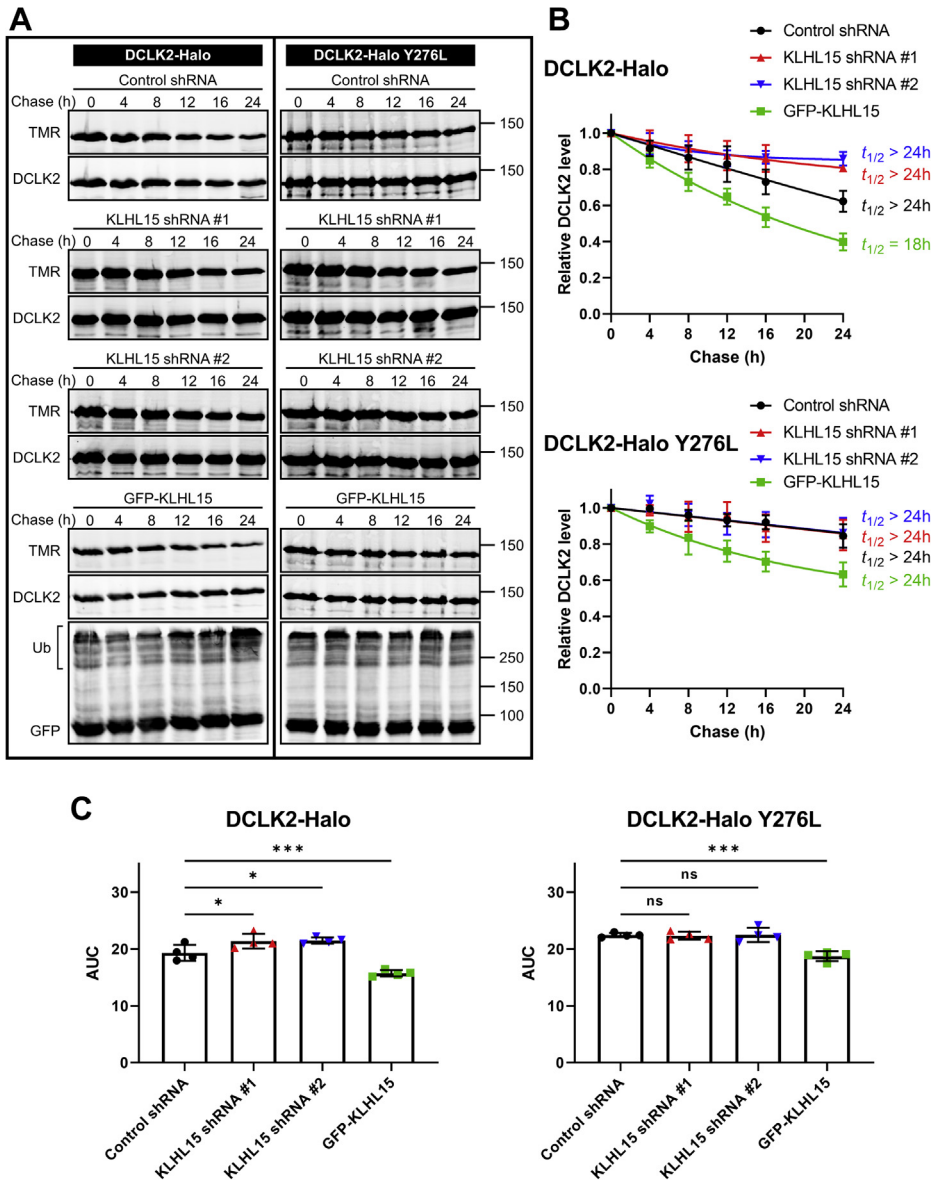


**Figure 7. KLHL15 facilitates DCLK2 protein degradation in a Y276-dependent manner.** HEK293T cells were cotransfected with DCLK2-HaloTag (WT or Y276L) and either the indicated shRNA plasmids or GFP-KLHL15. DCLK2-HaloTag was pulse labeled (30 min, 50 nM) with TMR fluorescent ligand and then chased with the non-fluorescent ligand 7-bromoheptanol for the indicated times before cell lysis. *A*, total lysate blots of cells expressing WT (*left*) or mutant (*right*) DCLK2-HaloTag were first imaged for TMR fluorescence and then immunoblotted for DCLK2 and GFP. Molecular mass marker positions are shown in kilodaltons. *B*, DCLK2 degradation was quantified by dividing TMR fluorescence by DCLK2 immunoblotting signals in the same lane (TMR/DCLK2) and normalizing to the zero time point. Data points are means ± SD from four independent transfections; half-lives ($t_{1/2}$) were determined from the shown one-phase decay curve fits. *C*, AUC was quantified from the decay curves in *B* and is plotted as individual data points and means ± SD from four repeated experiments. Data were analyzed by one-way ANOVA followed by Dunnett's post hoc tests for multiple comparisons to the control shRNA group. *$p < 0.05$, ***$p < 0.001$. AUC, area under the curve.

disease genes for neurodevelopmental disorders is currently circumstantial (66, 67). Although several studies identified *KLHL15* as an X-linked gene associated with various neurodevelopmental complications (8–11), a connection to DCX-domain proteins is not intuitively obvious, as their levels would be expected to increase, rather than decrease, in the absence of the E3 ligase. One could envision scenarios, however, in which *KLHL15* inactivation interferes with the normal developmental downregulation of DCX proteins and their replacement on microtubules with MAPs expressed later in development. Further studies involving animal models are required to investigate the interplay between KLHL15 and DCX proteins in the pathogenesis of neurodevelopmental disorders.

## Experimental procedures

### *Cell culture and transfection*

COS-1 and HEK293T cells were cultured at 37 °C and 5% $CO_2$ in Dulbecco's modified Eagle medium (Gibco) supplemented with 10% fetal bovine serum (Atlanta Biologicals) and 1% (v/v) GlutaMax (Gibco). Cells were grown to 60% confluency on collagen-coated plates and transfected using Lipofectamine 2000 (Invitrogen) following the manufacture's

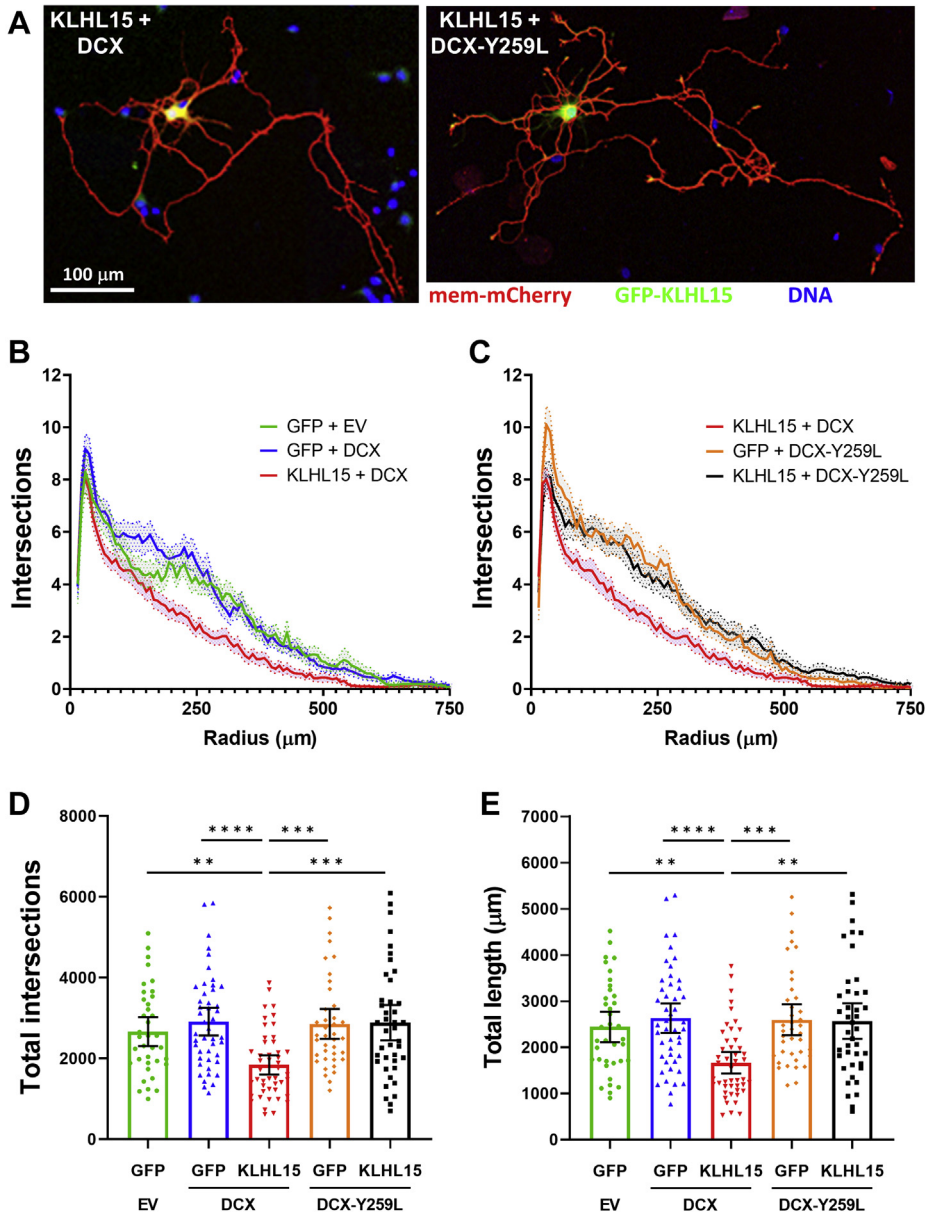


**Figure 8. KLHL15 antagonizes dendrite outgrowth of hippocampal neurons via DCX.** *A*, representative images of hippocampal neurons from E18 rat embryos transfected with membrane-targeted mCherry (*red*), GFP-KLHL15 (*green*), and either WT DCX (*left*) or Y259L mutant (*right*); nuclei are labeled *blue*. *B* and *C*, plots of numbers of dendrite intersections with concentric circles (steps of 7.5 μm starting 15 μm from the soma) obtained by Sholl analysis of traced dendrites. For clarity, the five transfection conditions were separated into two graphs with KLHL15 + DCX shown in both. *D* and *E*, plots of the total number of dendrite intersections from the Sholl analysis (*D*) and total dendrite length (*E*). Shown are means ± 95% CI (as well as individual data points in *D* and *E*) of 37 to 47 neurons from three or four cultures per transfection condition. Data were analyzed by Kruskal–Wallis followed by Dunn's multiple comparisons tests. $^{**}p < 0.01$, $^{***}p < 0.001$, and $^{****}p < 0.0001$.

protocol for transient transfection of adhered cells. Primary hippocampal cultures were prepared from embryonic day 18 (E18) Sprague Dawley rats (Harlan) as described previously (41). Hippocampi were dissected and pooled in ice-cold HEPES-buffered neurobasal and then incubated in HBSS containing trypsin (1.5 mg/ml) at 37 °C for 12 min. The tissues were washed three times with HBSS before cells were dissociated by trituration. Cells were plated in Neurobasal complete (Neurobasal media (Gibco), 2% B27 supplement, 10 mM HEPES, and 0.25% GlutaMax) and 5% horse serum on poly-L-lysine-coated plates. Medium was changed to serum-free Neurobasal complete after 4 h of incubation. Cells were maintained at 37 °C in a humidified environment of 95% air/5% $CO_2$ with half the media changed with fresh media twice a week (41).

### *Plasmids*

The green fluorescent protein (GFP)-tagged KLHL15 replacement plasmids, control, and KLHL15- and B'*β*-directed small hairpin RNAs (shRNAs) were previously described (15). The mouse DCX cDNA (transcript variant 3, NM_001110224.1) was obtained from Origene in the pCMV6 vector that also incorporates C-terminal Myc and FLAG tags (Myc-FLAG). The

human cDNAs for DCLK1 (NM_001330072.2), DCLK2 (BC032726.1), and DCLK3 (NM_033403.1) were obtained from DNASU and subcloned into pCMV6-Myc-FLAG. For pulse-chase experiments, DCX and DCLK cDNAs were transferred into a pHT-C (Promega)-derived vector that expresses C-terminal HaloTag (41). Missense mutations, chimeras, and truncations of DCX and DCLKs were generated by PCR following standard protocols (15). The DCX-HaloTag-$His_6$ fusion cDNA was also subcloned into the bacterial expression plasmid pET-21b(+) using compatible restriction sites. Plasmids expressing GFP-Drp1, GFP-B$\beta$2 RR168EE, FLAG-RIβ, GST-$KLHL15_{Kelch}$, GST-$KLHL9_{Kelch}$, HA-Cul3, HA-Cul3ΔRoc, and HA-ubiquitin were described previously (15). All constructs were verified by sequencing by the Iowa Institute of Human Genetics Genomics Division.

### *Antibodies and reagents*

The commercially sourced primary antibodies used in this study include rabbit anti-GFP (ab290, Abcam), mouse anti-GFP (N86/8) (75-131, NeuroMab), mouse anti-FLAG (M2) (F3165, Sigma), rabbit anti-DYKDDDDK (FLAG) Tag (2368, Cell Signaling), mouse anti-Doublecortin (E-6) (sc-271390, Santa Cruz), rabbit anti-Doublecortin (4604, Cell Signaling), rabbit anti-DCLK1/DCAMKL1 (D2U3L) (62257, Cell Signaling), rabbit anti-DCLK2 (ab106639, Abcam), goat anti-GST (27-4577-01, Amersham), mouse anti-V5-Tag (46-0705, Invitrogen), mouse anti-Myc-Tag (9B11) (2276, Cell Signaling), rabbit anti-HA-Tag (C29F4) (3724, Cell Signaling), and rabbit anti-ubiquitin (3933, Cell Signaling). The rabbit polyclonal antibody against B'$\beta$ was described previously (16). Secondary antibodies were IRDye 680RD goat anti-mouse IgG (926-68070, LI-COR Biosciences), IRDye 800CW goat anti-rabbit IgG (926-32211, LI-COR Biosciences), IRDye 680RD donkey anti-mouse IgG (926-68072, LI-COR Biosciences), IRDye 800CW donkey anti-rabbit IgG (926-32213, LI-COR Biosciences), IRDye 680RD donkey anti-goat IgG (926-68074, LI-COR Biosciences), and Superclonal goat anti-rabbit IgG, horseradish peroxidase conjugate (A27036, Invitrogen).

The chemical reagents used in this study were listed as follows: MG132 (C2211, Sigma), MLN4924 (5.05477.0001, Millipore), HaloTag TMR ligand (G8251, Promega), 7-Bromo-1-heptanol (H54762, Alfa Aesar), EZview Red anti-FLAG M2 affinity gel (F2426, Sigma), GFP-nanobody agarose resin (143093, University of Iowa Biomedical Research Store), Glutathione-Superflow resin (635607, Takara), His60 Ni Superflow Resin (635660, Takara), lysozyme from chicken egg white (L6876, Sigma), recombinant human UBE1 (E-305, Boston Biochem), recombinant human UbcH5a/UBE2D1 (E2-616, Boston Biochem), Myc-ubiquitin (U-115, Boston Biochem), ubiquitin aldehyde (U-201, Boston Biochem), creatine phosphokinase from rabbit muscle (C3755, Sigma), sodium creatine phosphate dibasic tetrahydrate (27920, Sigma), ATP (R0441, Thermo Scientific), human BDNF (2837, Tocris), PACAP-38 (4031157, Bachem), poly-L-lysine hydrobromide (OKK-3056, Peptides International), and Western Lightning Ultra (NEL113001EA, PerkinElmer).

### *Dual luciferase reporter assays*

Primary rat hippocampal cultures were plated at 50,000 cells per well in 48-well plates and transfected on DIV 9 (day *in vitro*) using NeuroMag magnetic beads. For the transfection, KLHL15, B'$\beta$ or GFP, and empty vector control or shRNA-expressing plasmid were combined with the PathDetect Elk1 trans-reporting system (Agilent) and an SV40 promoter-driven NanoLuciferase plasmid (pNL1.1, Promega) for normalization. On DIV 13, cultures were treated with either media or media containing BDNF (25 ng/ml final) or PACAP (10 nM final) and assayed 3 h later with the Nano-Glo Dual-Luciferase Reporter System (N1630, Promega) on a Berthold Sirius luminometer to quantify ERK activation.

### *Immunoprecipitation and immunoblot analyses*

Immunoprecipitation (IP) was carried out as previously described (15). Briefly, COS-1 cells were seeded and grown on collagen-coated 6-well plates followed by transfection. Cells were lysed in IP buffer (20 mM Tris, pH 7.5, 150 mM NaCl, 1% Triton X-100, 1 mM EDTA, 1 mM EGTA, 1 mM benzamidine, 1 mM PMSF, and 1 μg/ml leupeptin) and rotated at 4 °C for 30 min to allow sufficient solubilization. The total lysates were centrifuged at 13,000*g* for 10 min to separate the cytosol from insoluble fraction and cell debris. Ten percent of the supernatant was sampled out as input; the remainder was then subjected to either FLAG-IP or GFP-IP using pre-equilibrated anti-FLAG M2 affinity gel or GFP-nanobody agarose resin (10–15 μl bead volume per reaction), respectively, for 2 h rotating at 4 °C. Beads were washed four times by centrifugation in lysis buffer and eluted by boiling in 2× Laemmli sample buffer for 5 min. For *in vitro* ubiquitination assays, Cul3–KLHL15 E3 ubiquitin ligase complex was immunopurified by GFP-IP from HEK293T cells coexpressing GFP-KLHL15 and HA-Cul3. Precipitates were washed four times with 50 mM NaCl, 50 mM HEPES, 10% glycerol, 0.1% Tween 20, and 20 mM Tris, pH 7.5. The immobilized Cul3–KLHL15 E3 complex integrity was verified by immunoblotting and immediately used for *in vitro* ubiquitination assays. Samples were separated on 10% SDS-PAGE gels, electrotransferred to nitrocellulose membrane (GE Healthcare), and immunoblotted as indicated. Generally, proteins were visualized by using species-specific fluorescent secondary antibodies and a LI-COR Odyssey infrared scanner for dual-color detection. Immunoblotting signals were quantified by densitometry using the gel analysis plugin of ImageJ (National Institutes of Health).

### *Purification of bacterially expressed proteins*

GST, GST-$KLHL9_{Kelch}$, GST-$KLHL15_{Kelch}$, DCX-HaloTag-$His_6$, DCX-HaloTag-$His_6$ Y259L, and HaloTag-$His_6$ were expressed in *E. coli* BL21(DE3) cells (200131, Agilent) and purified according to standard procedures as previously described (15). Briefly, bacterial cells were grown at 37 °C, 200 rpm to OD ∼0.8 and induced with 500 μM IPTG for 6 to 8 h. Cells were pelleted by centrifugation at 3000 rpm for 15 min and lysed in 50 mM Tris, pH 7.5, 150 mM NaCl, 2 mM

benzamidine, 1 mM PMSF, and 1 mg/ml lysozyme for 30 min to complete lysis, followed by a total of 2 min sonication (15 s on, 45 s off; 8 rounds on ice). Samples were centrifuged at 15,000 rpm for 15 min and the supernatant was then applied to the appropriate resin following the manufacture's protocol. The $His_6$-tagged proteins were eluted with 250 mM imidazole and dialyzed into the desired buffer while the GST proteins remained immobilized on glutathione resin. Purified proteins were quantified by Coomassie staining with bovine serum albumin standards within the linear range and were utilized immediately.

### *GST pulldown assays*

Whole brains were rapidly dissected from embryos (E18) of Sprague-Dawley rats following decapitation, flash frozen in liquid nitrogen, and stored at −80 °C until use. For whole brain lysates, frozen tissues were pulverized and homogenized in lysis buffer containing 25 mM Tris, pH 7.5, 50 mM NaCl, 0.5% Triton X-100, 2 mM DTT, 0.5 mM EDTA, 1 mM benzamidine, 1 mM PMSF, and 1 μg/ml leupeptin. Homogenates were sonicated to shear DNA and cleared by centrifugation (15 min at 20,000*g*). A portion of the brain homogenate supernatant was added directly to 4× Laemmli buffer to provide an input sample. GST pulldown assays were performed by mixing 60 to 100 μl whole brain lysates with ∼30 μg immobilized GST proteins for 2 h rotating at 4 °C. Glutathione resins were washed four times by centrifugation in lysis buffer and eluted in 2× Laemmli sample buffer. Protein samples were subjected to SDA-PAGE and immunoblotting with the indicated antibodies.

### *In-cell ubiquitination assays*

About 24 to 36 h post transfection, COS-1 cells were treated with 25 μM MG132 (from 50 mM stock in DMSO) for 8 to 12 h before lysis to permit sufficient proteasomal inhibition. A final concentration of 2 μM MLN4924 (from 10 mM stock in DMSO) was added alone or in combination with MG132 for NEDD8-activating enzyme inhibition. Cytosolic fraction was then subject to FLAG-IP as described above and immunoblotted for DCX for DCX-specific ubiquitination. The effectiveness of MG132 was confirmed by the accumulation of DCX polyubiquitination and/or stabilization of steady-state protein level in the presence of MG132 in cells expressing FLAG-DCX alone. DCX immunoblotting signals were visualized by quantitative fluorescent imaging (LI-COR) using species-specific secondary antibodies to avoid detection of heavy chain and light chain of denatured antibodies during IP.

### In vitro *ubiquitination assays*

*In vitro* ubiquitination assays were done as previously described (68), but modified for 48-well plates. Briefly, the ubiquitination reaction mixture contained 125 ng of E1 enzyme (Boston Biochem), 250 ng of E2 enzyme (Boston Biochem), immunopurified Cul3–KLHL15 E3 complex, 10 μg of Myc-ubiquitin (Boston Biochem), 1 μM ubiquitin aldehyde (Boston Biochem), 10 mM $MgCl_2$, 2 mM DTT, 10 mM creatine phosphate (Sigma), 0.5 mg/ml creatine phosphokinase (Sigma), and 20 μg of purified proteins including DCX-HaloTag-$His_6$ (WT or Y259L) or Halo-$His_6$ as control protein. The ubiquitination reactions were diluted to a final volume of 0.25 ml in 50 mM HEPES, pH 7.5, initiated upon addition of 5 mM ATP (Thermo Scientific), and incubated for up to 2 h at 37 °C on a titer plate shaker (constant speed 3, Lab-Line Instruments, Inc). Thirty-microliter reaction mixtures were sampled at the indicated times and immediately terminated in 4× Laemmli buffer. Proteins were then resolved on 8% gels by SDS-PAGE, and ubiquitinated proteins were detected by immunoblotting with Myc-Tag antibody.

Relative DCX ubiquitination *in vitro* was quantified by dividing Myc-Tag signals by DCX signals and GFP (KLHL15) signals in the same lane and normalizing to the zero time point (set to 1). The enzymatic kinetics was plotted in Michaelis–Menten model using GraphPad Prism.

### *HaloTag turnover assays*

HaloTag-based turnover assays were conducted following a pulse-chase protocol as previously reported (41). Briefly, HEK293T cells were transfected with HaloTag constructs with KLHL15-targeted shRNA or a control shRNA. For gain-of-function study, HaloTag construct was cotransfected with GFP-KLHL15 replacement vector or a GFP-control vector. About 24 to 36 h post transfection, cells were incubated with 50 nM fluorescent cell-permeant HaloTag TMR ligand for 30 min at 37 °C to allow maximal labeling. Then TMR-containing media was removed and replaced with media containing 10 μM 7-bromoheptanol blocker for the indicated times. Assays were terminated by cell lysis in SDS sample buffer, and HaloTag proteins were separated by SDS-PAGE. TMR fluorescence was visualized by Sapphire Biomolecular Imager using a Cy3 filter (Azure Biosystems), and total DCX (or DCLK) protein was subsequently probed with the indicated antibodies. Relative DCX (or DCLK) protein levels were quantified by dividing TMR fluorescence signals by individual immunoblotting signals in the same lane and normalizing to the zero time point (set to 1). Half-lives ($t_{1/2}$) were calculated from the one-phase decay model using GraphPad Prism.

### *Dendrite outgrowth assays*

Primary rat hippocampal cultures from E18 embryos were plated at 50,000 cells per ml in cover glass bottomed chambers and plates (C8-1.5H-N and P24-1.5H-N, Cellvis). At DIV 2, cultures were transfected with 0.2% Lipofectamine 2000 and the following DNA constructs at these ratios: 20% Lck-2V5-mCherry (plasma membrane targeted, also containing two V5 tags), 40% empty vector (EV), DCX-WT or DCX-Y259L, and 40% EGFP or GFP-KLHL15. On DIV 5, cultures were fixed in 4% paraformaldehyde and intrinsic fluorescence was amplified with antibodies to GFP and the V5 tag and appropriate fluorescent secondary antibodies. Image stacks (11 focal planes at 1-μm intervals) were acquired using the 10× objective of a Keyence BZ-X800E microscope and converted

to maximum intensity projections. Dendrites were traced semiautomatically using the ImageJ plugin SNT, and traces were analyzed for length (total pixel number) and with the Sholl Analysis plugin for intersections with concentric circles (7.5 μm apart, starting 15 μm from the cell body). All analyses were performed blinded to the transfection conditions.

### *Statistical analysis*

Statistical analyses were performed using GraphPad Prism 8 with tests listed in the figure captions. The robust outlier removal (ROUT) method of removing outliers was used at Q = 1% prior to normalization of data and significance levels are abbreviated as follows: $^{*}p < 0.05$, $^{**}p < 0.01$, $^{***}p < 0.001$, and $^{****}p < 0.0001$.

## Data availability

All data are contained within the manuscript.

*Author contributions*—J. S., R. A. M., and S. S. conceptualization; J. S., R. A. M., and S. S. writing; J. S., R. A. M., and A. Y. U. investigation; S. S. resources; S. S. supervision; S. S. funding acquisition; S. S. project administration.

*Funding and additional information*—This work was supported by National Institutes of Health grants DK116624, MH115673, MH113352 (to S. S.). The content is solely the responsibility of the authors and does not necessarily represent the official views of the National Institutes of Health. Additional support to S. S. was provided by Jordan's Guardian Angels, the Roy J. Carver Charitable Trust, and Iowa Neuroscience Institute. We also acknowledge support by the Genomics Division of the University of Iowa Carver College of Medicine.

*Conflict of interest*—The authors declare that they have no conflicts of interest with the contents of this article.

*Abbreviations*—The abbreviations used are: AUC, area under the curve; BDNF, brain-derived neurotrophic factor; Cul3, cullin3; CRL, cullin-RING ligase; DCLK, doublecortin-like kinase; DCX, doublecortin; ERK, extracellular signal-regulated kinase; GFP, green fluorescent protein; GST, glutathione-*S*-transferase; IP, immunoprecipitation; KLHL, Kelch-like; MAP, microtubule-associated protein; PACAP, pituitary adenylate cyclase-activating polypeptide; PP2A, protein phosphatase 2A; TMR, tetramethyl rhodamine; Trk, tropomyosin-related kinase; XLID, X-linked intellectual disability.

## References

1. Vucic, D., Dixit, V. M., and Wertz, I. E. (2011) Ubiquitylation in apoptosis: a post-translational modification at the edge of life and death. *Nat. Rev. Mol. Cell Biol.* **12**, 439–452
2. Cheon, S., Dean, M., and Chahrour, M. (2019) The ubiquitin proteasome pathway in neuropsychiatric disorders. *Neurobiol. Learn. Mem.* **165**, 106791
3. Hegde, A. N., and Upadhya, S. C. (2007) The ubiquitin-proteasome pathway in health and disease of the nervous system. *Trends Neurosci.* **30**, 587–595
4. Groen, E. J. N., and Gillingwater, T. H. (2015) UBA1: at the crossroads of ubiquitin homeostasis and neurodegeneration. *Trends Mol. Med.* **21**, 622–632
5. Upadhyay, A., Joshi, V., Amanullah, A., Mishra, R., Arora, N., Prasad, A., and Mishra, A. (2017) E3 ubiquitin ligases neurobiological mechanisms: development to degeneration. *Front. Mol. Neurosci.* **10**, 151
6. Louros, S. R., and Osterweil, E. K. (2016) Perturbed proteostasis in autism spectrum disorders. *J. Neurochem.* **139**, 1081–1092
7. Upadhyay, A., Amanullah, A., Chhangani, D., Mishra, R., and Mishra, A. (2015) Selective multifaceted E3 ubiquitin ligases barricade extreme defense: potential therapeutic targets for neurodegeneration and ageing. *Ageing Res. Rev.* **24**, 138–159
8. Hu, H., Haas, S. A., Chelly, J., Van Esch, H., Raynaud, M., de Brouwer, A. P., Weinert, S., Froyen, G., Frints, S. G., Laumonnier, F., Zemojtel, T., Love, M. I., Richard, H., Emde, A. K., Bienek, M., *et al.* (2016) X-exome sequencing of 405 unresolved families identifies seven novel intellectual disability genes. *Mol. Psychiatry* **21**, 133–148
9. Mignon-Ravix, C., Cacciagli, P., Choucair, N., Popovici, C., Missirian, C., Milh, M., Megarbane, A., Busa, T., Julia, S., Girard, N., Badens, C., Sigaudy, S., Philip, N., and Villard, L. (2014) Intragenic rearrangements in X-linked intellectual deficiency: results of a-CGH in a series of 54 patients and identification of TRPC5 and KLHL15 as potential XLID genes. *Am. J. Med. Genet. A.* **164A**, 1991–1997
10. Schumann, M., Hofmann, A., Krutzke, S. K., Hilger, A. C., Marsch, F., Stienen, D., Gembruch, U., Ludwig, M., Merz, W. M., and Reutter, H. (2016) Array-based molecular karyotyping in fetuses with isolated brain malformations identifies disease-causing CNVs. *J. Neurodev. Disord.* **8**, 11
11. Karaca, E., Harel, T., Pehlivan, D., Jhangiani, S. N., Gambin, T., Coban Akdemir, Z., Gonzaga-Jauregui, C., Erdin, S., Bayram, Y., Campbell, I. M., Hunter, J. V., Atik, M. M., Van Esch, H., Yuan, B., Wiszniewski, W., *et al.* (2015) Genes that affect brain structure and function identified by rare variant analyses of mendelian neurologic disease. *Neuron* **88**, 499–513
12. Shi, X., Xiang, S., Cao, J., Zhu, H., Yang, B., He, Q., and Ying, M. (2019) Kelch-like proteins: physiological functions and relationships with diseases. *Pharmacol. Res.* **148**, 104404
13. Dhanoa, B. S., Cogliati, T., Satish, A. G., Bruford, E. A., and Friedman, J. S. (2013) Update on the Kelch-like (KLHL) gene family. *Hum. Genomics* **7**, 13
14. Gupta, V. A., and Beggs, A. H. (2014) Kelch proteins: emerging roles in skeletal muscle development and diseases. *Skelet. Muscle* **4**, 11
15. Oberg, E. A., Nifoussi, S. K., Gingras, A. C., and Strack, S. (2012) Selective proteasomal degradation of the B'beta subunit of protein phosphatase 2A by the E3 ubiquitin ligase adaptor Kelch-like 15. *J. Biol. Chem.* **287**, 43378–43389
16. Saraf, A., Virshup, D. M., and Strack, S. (2007) Differential expression of the B'beta regulatory subunit of protein phosphatase 2A modulates tyrosine hydroxylase phosphorylation and catecholamine synthesis. *J. Biol. Chem.* **282**, 573–580
17. McCright, B., and Virshup, D. M. (1995) Identification of a new family of protein phosphatase 2A regulatory subunits. *J. Biol. Chem.* **270**, 26123–26128
18. Martens, E., Stevens, I., Janssens, V., Vermeesch, J., Gotz, J., Goris, J., and Van Hoof, C. (2004) Genomic organisation, chromosomal localisation tissue distribution and developmental regulation of the PR61/B' regulatory subunits of protein phosphatase 2A in mice. *J. Mol. Biol.* **336**, 971–986
19. Fukunaga, K., Muller, D., Ohmitsu, M., Bako, E., DePaoli-Roach, A. A., and Miyamoto, E. (2000) Decreased protein phosphatase 2A activity in hippocampal long-term potentiation. *J. Neurochem.* **74**, 807–817
20. Bidinosti, M., Botta, P., Kruttner, S., Proenca, C. C., Stoehr, N., Bernhard, M., Fruh, I., Mueller, M., Bonenfant, D., Voshol, H., Carbone, W., Neal, S. J., McTighe, S. M., Roma, G., Dolmetsch, R. E., *et al.* (2016) CLK2 inhibition ameliorates autistic features associated with SHANK3 deficiency. *Science* **351**, 1199–1203
21. Brandt, N., Franke, K., Johannes, S., Buck, F., Harder, S., Hassel, B., Nitsch, R., and Schumacher, S. (2008) B56beta, a regulatory subunit of protein phosphatase 2A, interacts with CALEB/NGC and inhibits CALEB/NGC-mediated dendritic branching. *FASEB J.* **22**, 2521–2533
22. Van Kanegan, M. J., and Strack, S. (2009) The protein phosphatase 2A regulatory subunits B'beta and B'delta mediate sustained TrkA

neurotrophin receptor autophosphorylation and neuronal differentiation. *Mol. Cell Biol* **29**, 662–674
23. Ferretti, L. P., Himmels, S. F., Trenner, A., Walker, C., von Aesch, C., Eggenschwiler, A., Murina, O., Enchev, R. I., Peter, M., Freire, R., Porro, A., and Sartori, A. A. (2016) Cullin3-KLHL15 ubiquitin ligase mediates CtIP protein turnover to fine-tune DNA-end resection. *Nat. Commun.* **7**, 12628
24. Ge, X., Kwok, P. Y., and Shieh, J. T. (2015) Prioritizing genes for X-linked diseases using population exome data. *Hum. Mol. Genet.* **24**, 599–608
25. Reiner, O., Coquelle, F. M., Peter, B., Levy, T., Kaplan, A., Sapir, T., Orr, I., Barkai, N., Eichele, G., and Bergmann, S. (2006) The evolving doublecortin (DCX) superfamily. *BMC Genomics* **7**, 188
26. Fourniol, F., Perderiset, M., Houdusse, A., and Moores, C. (2013) Structural studies of the doublecortin family of MAPs. *Methods Cell Biol.* **115**, 27–48
27. Coquelle, F. M., Levy, T., Bergmann, S., Wolf, S. G., Bar-El, D., Sapir, T., Brody, Y., Orr, I., Barkai, N., Eichele, G., and Reiner, O. (2006) Common and divergent roles for members of the mouse DCX superfamily. *Cell Cycle* **5**, 976–983
28. Dijkmans, T. F., van Hooijdonk, L. W., Fitzsimons, C. P., and Vreugdenhil, E. (2010) The doublecortin gene family and disorders of neuronal structure. *Cent. Nerv Syst. Agents Med. Chem.* **10**, 32–46
29. Reiner, O. (2013) LIS1 and DCX: implications for brain development and human disease in relation to microtubules. *Scientifica (Cairo)* **2013**, 393975
30. Hehr, U., Uyanik, G., Aigner, L., Couillard-Despres, S., and Winkler, J. (1993) DCX-related disorders. In: Adam, M. P., Ardinger, H. H., Pagon, R. A., Wallace, S. E., Bean, L. J. H., Stephens, K., Amemiya, A., eds. *GeneReviews((R))*, University of Washington. Seattle, WA
31. Lin, P. T., Gleeson, J. G., Corbo, J. C., Flanagan, L., and Walsh, C. A. (2000) DCAMKL1 encodes a protein kinase with homology to doublecortin that regulates microtubule polymerization. *J. Neurosci.* **20**, 9152–9161
32. Edelman, A. M., Kim, W. Y., Higgins, D., Goldstein, E. G., Oberdoerster, M., and Sigurdson, W. (2005) Doublecortin kinase-2, a novel doublecortin-related protein kinase associated with terminal segments of axons and dendrites. *J. Biol. Chem.* **280**, 8531–8543
33. Shin, E., Kashiwagi, Y., Kuriu, T., Iwasaki, H., Tanaka, T., Koizumi, H., Gleeson, J. G., and Okabe, S. (2013) Doublecortin-like kinase enhances dendritic remodelling and negatively regulates synapse maturation. *Nat. Commun.* **4**, 1440
34. Deuel, T. A., Liu, J. S., Corbo, J. C., Yoo, S. Y., Rorke-Adams, L. B., and Walsh, C. A. (2006) Genetic interactions between doublecortin and doublecortin-like kinase in neuronal migration and axon outgrowth. *Neuron* **49**, 41–53
35. Koizumi, H., Tanaka, T., and Gleeson, J. G. (2006) Doublecortin-like kinase functions with doublecortin to mediate fiber tract decussation and neuronal migration. *Neuron* **49**, 55–66
36. Tanaka, T., Koizumi, H., and Gleeson, J. G. (2006) The doublecortin and doublecortin-like kinase 1 genes cooperate in murine hippocampal development. *Cereb. Cortex* **16 Suppl 1**, i69–i73
37. Kerjan, G., Koizumi, H., Han, E. B., Dube, C. M., Djakovic, S. N., Patrick, G. N., Baram, T. Z., Heinemann, S. F., and Gleeson, J. G. (2009) Mice lacking doublecortin and doublecortin-like kinase 2 display altered hippocampal neuronal maturation and spontaneous seizures. *Proc. Natl. Acad. Sci. U. S. A.* **106**, 6766–6771
38. Vaudry, D., Stork, P. J., Lazarovici, P., and Eiden, L. E. (2002) Signaling pathways for PC12 cell differentiation: making the right connections. *Science* **296**, 1648–1649
39. Shu, T., Tseng, H. C., Sapir, T., Stern, P., Zhou, Y., Sanada, K., Fischer, A., Coquelle, F. M., Reiner, O., and Tsai, L. H. (2006) Doublecortin-like kinase controls neurogenesis by regulating mitotic spindles and M phase progression. *Neuron* **49**, 25–39
40. Ohmae, S., Takemoto-Kimura, S., Okamura, M., Adachi-Morishima, A., Nonaka, M., Fuse, T., Kida, S., Tanji, M., Furuyashiki, T., Arakawa, Y., Narumiya, S., Okuno, H., and Bito, H. (2006) Molecular identification and characterization of a family of kinases with homology to Ca2+/calmodulin-dependent protein kinases I/IV. *J. Biol. Chem.* **281**, 20427–20439
41. Merrill, R. A., Song, J., Kephart, R. A., Klomp, A. J., Noack, C. E., and Strack, S. (2019) A robust and economical pulse-chase protocol to measure the turnover of HaloTag fusion proteins. *J. Biol. Chem.* **294**, 16164–16171
42. Yap, C. C., Digilio, L., McMahon, L., Roszkowska, M., Bott, C. J., Kruczek, K., and Winckler, B. (2016) Different doublecortin (DCX) patient Alleles show distinct phenotypes in cultured neurons: evidence for divergent loss-of-function and "OFF-pathway" cellular mechanisms. *J. Biol. Chem.* **291**, 26613–26626
43. Yamada, T., Yang, Y., and Bonni, A. (2013) Spatial organization of ubiquitin ligase pathways orchestrates neuronal connectivity. *Trends Neurosci.* **36**, 218–226
44. Lip, P. Z., Demasi, M., and Bonatto, D. (2017) The role of the ubiquitin proteasome system in the memory process. *Neurochem. Int.* **102**, 57–65
45. Rape, M. (2018) Ubiquitylation at the crossroads of development and disease. *Nat. Rev. Mol. Cell Biol.* **19**, 59–70
46. Layfield, R., Cavey, J. R., and Lowe, J. (2003) Role of ubiquitin-mediated proteolysis in the pathogenesis of neurodegenerative disorders. *Ageing Res. Rev.* **2**, 343–356
47. Zheng, N., and Shabek, N. (2017) Ubiquitin ligases: structure, function, and regulation. *Annu. Rev. Biochem.* **86**, 129–157
48. Deshaies, R. J., and Joazeiro, C. A. (2009) RING domain E3 ubiquitin ligases. *Annu. Rev. Biochem.* **78**, 399–434
49. Lydeard, J. R., Schulman, B. A., and Harper, J. W. (2013) Building and remodelling Cullin-RING E3 ubiquitin ligases. *EMBO Rep.* **14**, 1050–1061
50. George, A. J., Hoffiz, Y. C., Charles, A. J., Zhu, Y., and Mabb, A. M. (2018) A comprehensive atlas of E3 ubiquitin ligase mutations in neurological disorders. *Front. Genet.* **9**, 29
51. Moores, C. A., Perderiset, M., Francis, F., Chelly, J., Houdusse, A., and Milligan, R. A. (2004) Mechanism of microtubule stabilization by doublecortin. *Mol. Cell* **14**, 833–839
52. Bechstedt, S., and Brouhard, G. J. (2012) Doublecortin recognizes the 13-protofilament microtubule cooperatively and tracks microtubule ends. *Dev. Cell* **23**, 181–192
53. Bechstedt, S., Lu, K., and Brouhard, G. J. (2014) Doublecortin recognizes the longitudinal curvature of the microtubule end and lattice. *Curr. Biol.* **24**, 2366–2375
54. Francis, F., Koulakoff, A., Boucher, D., Chafey, P., Schaar, B., Vinet, M. C., Friocourt, G., McDonnell, N., Reiner, O., Kahn, A., McConnell, S. K., Berwald-Netter, Y., Denoulet, P., and Chelly, J. (1999) Doublecortin is a developmentally regulated, microtubule-associated protein expressed in migrating and differentiating neurons. *Neuron* **23**, 247–256
55. Gleeson, J. G., Lin, P. T., Flanagan, L. A., and Walsh, C. A. (1999) Doublecortin is a microtubule-associated protein and is expressed widely by migrating neurons. *Neuron* **23**, 257–271
56. Tanaka, T., Serneo, F. F., Tseng, H. C., Kulkarni, A. B., Tsai, L. H., and Gleeson, J. G. (2004) Cdk5 phosphorylation of doublecortin ser297 regulates its effect on neuronal migration. *Neuron* **41**, 215–227
57. Friocourt, G., Kappeler, C., Saillour, Y., Fauchereau, F., Rodriguez, M. S., Bahi, N., Vinet, M. C., Chafey, P., Poirier, K., Taya, S., Wood, S. A., Dargemont, C., Francis, F., and Chelly, J. (2005) Doublecortin interacts with the ubiquitin protease DFFRX, which associates with microtubules in neuronal processes. *Mol. Cell Neurosci* **28**, 153–164
58. Couillard-Despres, S., Winner, B., Karl, C., Lindemann, G., Schmid, P., Aigner, R., Laemke, J., Bogdahn, U., Winkler, J., Bischofberger, J., and Aigner, L. (2006) Targeted transgene expression in neuronal precursors: watching young neurons in the old brain. *Eur. J. Neurosci.* **24**, 1535–1545
59. Fung, S. J., Joshi, D., Allen, K. M., Sivagnanasundaram, S., Rothmond, D. A., Saunders, R., Noble, P. L., Webster, M. J., and Weickert, C. S. (2011) Developmental patterns of doublecortin expression and white matter neuron density in the postnatal primate prefrontal cortex and schizophrenia. *PLoS One* **6**, e25194
60. Friocourt, G., Koulakoff, A., Chafey, P., Boucher, D., Fauchereau, F., Chelly, J., and Francis, F. (2003) Doublecortin functions at the extremities of growing neuronal processes. *Cereb. Cortex* **13**, 620–626

61. Tint, I., Jean, D., Baas, P. W., and Black, M. M. (2009) Doublecortin associates with microtubules preferentially in regions of the axon displaying actin-rich protrusive structures. *J. Neurosci.* **29**, 10995–11010
62. Koizumi, H., Higginbotham, H., Poon, T., Tanaka, T., Brinkman, B. C., and Gleeson, J. G. (2006) Doublecortin maintains bipolar shape and nuclear translocation during migration in the adult forebrain. *Nat. Neurosci.* **9**, 779–786
63. Yoshihara, S., Takahashi, H., Nishimura, N., Kinoshita, M., Asahina, R., Kitsuki, M., Tatsumi, K., Furukawa-Hibi, Y., Hirai, H., Nagai, T., Yamada, K., and Tsuboi, A. (2014) Npas4 regulates Mdm2 and thus Dcx in experience-dependent dendritic spine development of newborn olfactory bulb interneurons. *Cell Rep.* **8**, 843–857
64. Cornell, B., Wachi, T., Zhukarev, V., and Toyo-Oka, K. (2016) Regulation of neuronal morphogenesis by 14-3-3epsilon (Ywhae) via the microtubule binding protein, doublecortin. *Hum. Mol. Genet.* **25**, 4405–4418
65. Cohen, D., Segal, M., and Reiner, O. (2008) Doublecortin supports the development of dendritic arbors in primary hippocampal neurons. *Dev. Neurosci.* **30**, 187–199
66. Smith, M., Woodroffe, A., Smith, R., Holguin, S., Martinez, J., Filipek, P. A., Modahl, C., Moore, B., Bocian, M. E., Mays, L., Laulhere, T., Flodman, P., and Spence, M. A. (2002) Molecular genetic delineation of a deletion of chromosome 13q12–>q13 in a patient with autism and auditory processing deficits. *Cytogenet. Genome Res.* **98**, 233–239
67. Meloche, J., Brunet, V., Gagnon, P. A., Lavoie, M. E., Bouchard, J. B., Nadaf, J., Majewski, J., Morin, C., and Laprise, C. (2020) Exome sequencing study of partial agenesis of the corpus callosum in men with developmental delay, epilepsy, and microcephaly. *Mol. Genet. Genomic Med.* **8**, e992
68. Ibeawuchi, S. R., Agbor, L. N., Quelle, F. W., and Sigmund, C. D. (2015) Hypertension-causing mutations in Cullin3 protein impair RhoA protein ubiquitination and augment the association with substrate adaptors. *J. Biol. Chem.* **290**, 19208–19217

**Jianing Song** is focused on understanding the molecular basis of E3 ubiquitin ligase in health and neurodevelopmental diseases. Despite the advancement of next-generation sequencing, the molecular underpinnings of the X-linked intellectual disability (XLID) caused by genetic mutations requires detailed study. He is interested in the ubiquitin-proteasome system (UPS) in neurons and the roles played by its key components, especially Kelch-like 15 (KLHL15), an E3 ubiquitin ligase adaptor protein and a clinically significant X-linked disease gene product.